The Journal of Chemical Physics

The spin-forbidden $a\,^4\Sigma^- - X\,^2\Pi_{1/2}$ transition of GeH detected in absorption using intracavity laser spectroscopy

Cite as: J. Chem. Phys. **148**, 204306 (2018); https://doi.org/10.1063/1.5017958
Submitted: 01 December 2017 . Accepted: 09 May 2018 . Published Online: 30 May 2018

Jack C. Harms, Leah C. O'Brien, and James J. O'Brien

The spin-forbidden $a\ ^4\Sigma^- – X\ ^2\Pi_{1/2}$ transition of GeH detected in absorption using intracavity laser spectroscopy

Jack C. Harms,[1] Leah C. O'Brien,[2,a)] and James J. O'Brien[1]
[1]*Department of Chemistry and Biochemistry and Center for Nanoscience, University of Missouri-St. Louis, Saint Louis, Missouri 63121, USA*
[2]*Department of Chemistry, Southern Illinois University Edwardsville, Edwardsville, Illinois 62026, USA*

(Received 1 December 2017; accepted 9 May 2018; published online 30 May 2018)

The $a\ ^4\Sigma^- – X\ ^2\Pi_{1/2}$ transition of GeH has been recorded in absorption for the first time using Intracavity Laser Spectroscopy (ILS). The GeH molecules were produced in a 0.40–0.60 A DC plasma discharge inside an aluminum hollow cathode, using 500 mTorr of Ar, 100 mTorr of H_2, and 200 mTorr of GeH_4. This cathode is located within the resonator cavity of a Coherent Verdi™ V-10 pumped dye laser. Effective path lengths for this series of measurements using the ILS method ranged from 2 to 7 km. Spectra were calibrated using the absorption spectrum of I_2 collected from an extracavity cell, the I_2 transmission spectrum from Salami and Ross, J. Mol. Spectrosc. **223**(1), 157 (2005) and PGOPHER's [C. M. Western, J. Quant. Spectrosc. Radiat. Transfer **186**, 221–242 (2016)] calibration feature. Differences in peak positions between calibrated experimental spectra and the reference data were on average less than $\pm 0.002\ cm^{-1}$. All eight branches expected to have appreciable intensity for the transition have been identified, and isotopologue splitting was observed in features of 5 of the 8 identified rotational branches. Molecular constants have been obtained for the $a\ ^4\Sigma^-$ states of ^{70}GeH (20.84% abundant), ^{72}GeH (27.54% abundant), and ^{74}GeH (36.28% abundant). The transitions were fit using PGOPHER, holding the ground state constants fixed to the values reported by Towle and Brown [Mol. Phys. **78**(2), 249 (1993)]. The constants for the $a\ ^4\Sigma^-$ state of ^{74}GeH determined by the fit are $T_0 = 16\,751.5524(13)\ cm^{-1}$, $B_0 = 6.764\,912(33)\ cm^{-1}$, $D_0 = 0.459\,60(17) \times 10^{-3}\ cm^{-1}$, $\lambda_{SS} = 9.7453(12)\ cm^{-1}$, $\lambda_D = 0.468(14) \times 10^{-3}\ cm^{-1}$, $\gamma = 0.077\,878(84)$, and $\gamma_S = -0.361(77) \times 10^{-3}\ cm^{-1}$. *Published by AIP Publishing.* https://doi.org/10.1063/1.5017958

I. INTRODUCTION

Germanium hydride is of interest because of its role in the production of germanium thin films produced from the dissociation of Germane, GeH_4.[1] The electronic structure of GeH has remained interesting to computational chemists because the comparison between experimentally determined values and theoretical predictions has shown the need for inclusion of several interactions to adequately model this simple molecular system.[1–5] The incorporation of correlation between the $3d^{10}$ electrons of Ge and spin-orbit coupling is necessary to accurately estimate the experimental transition energy and interpret the observations.[1] With added computational sophistication, the deviation of the estimated energy for the theoretical $B\ ^2\Sigma^+ – X\ ^2\Pi_r$ transition from the observed value went from −6%[2] to 0.6%.[1] In light of these most recent calculations, Li *et al.*[1] suggest that disagreements between the computational predictions and the previous experimental observations of the $a\ ^4\Sigma^- – X\ ^2\Pi_r$ transition merited further experimental measurements.

The spin-forbidden $a\ ^4\Sigma^- – X\ ^2\Pi_r$ transition was weakly observed by Kleman and Werhagen in 1953 in an emission from a King furnace using a germanium containing graphite boat and 0.5 atm of H_2.[6] The experimental photographs were not reproduced in the publication because "...[the transition's] weakness and the overlapping continuum do not permit of an acceptable reproduction." Budo and Kovacs[7] theoretically discussed $^4\Sigma – ^2\Pi$ transitions in a 1940 paper and predicted that the relative intensities of 8 of the 12 possible branches for a $^4\Sigma$-Hund's case (a) $^2\Pi_{1/2}$ transition will be non-zero, while 10 of the 12 possible transitions would have a non-zero relative intensity for a $^4\Sigma$–Hund's case (a) $^2\Pi_{3/2}$ transition. In their experimental study, Kleman and Werhagen were only able to identify 4 branches connecting to the $X\ ^2\Pi_{1/2}$ component and 5 branches connecting to the $X\ ^2\Pi_{3/2}$ component, and no isotopically resolved features were observed (natural abundances are ^{70}Ge 20.84%, ^{72}Ge 27.54%, ^{73}Ge 7.73%, ^{74}Ge 36.28%, and ^{76}Ge 7.61%). The identified branches were fit to obtain molecular constants for the $a\ ^4\Sigma^-$ state using a non-standard Hamiltonian developed by Budo. In 1966, Klynning[8] attempted to record the *a*-*X* transition in absorption, but was unsuccessful and instead reanalyzed the data of Kleman and Werhagen, fitting the term energies to Hougen's energy level expressions.[9] No other studies have reported experimental observations of this spin-forbidden transition.

In contrast to the $a\ ^4\Sigma^-$ state, the $X\ ^2\Pi_r$ ground state of GeH has been extensively studied experimentally using Laser Magnetic Resonance (LMR) and diode laser spectroscopy techniques to examine pure rotational, fine-structure, and vibrational transitions of GeH and GeD in the IR.[10–15] In

a)Author to whom correspondence should be addressed: lobrien@siue.edu. Tel.: 618-650-3562.

1993, Towle and Brown[16] performed a comprehensive fit of all available experimental data for the $X\ ^2\Pi_r$ ground state, which included transitions from all GeH isotopologues, excluding those involving tritium. The result is a set of molecular constants that effectively describe the ground state for the all isotopologues of the GeH molecule, not just the most abundant one, $^{74}Ge^1H$.

In this study, the $a\ ^4\Sigma^- – X\ ^2\Pi_{1/2}$ transition has been observed in absorption for the first time. All eight expected branches for this transition have been identified, and the data is in reasonable agreement with the theoretical predictions of Li *et al.*[1]

II. EXPERIMENTAL PROCEDURE

A. Intracavity laser spectrometer

The intracavity laser used for this study has been described elsewhere, and only a description of the modifications is provided here.[17] A schematic of the instrument is provided in Fig. 1(a), which shows a discharge plasma chamber with Brewster angle windows contained in the resonator chamber of a dye laser. A Coherent Verdi^{TM} V-10 Laser operating at 532 nm and set to 0.50–1.50 W is used to pump 3 mM of 4-dicyanomethylene-2-methyl-6-(p-dimethylaminostyryl)-4H-pyran (DCM) laser dye in 2-phenoxy-ethanol (EPH), circulated through a Spectra Physics sapphire nozzle at a pressure of ~80 psi. This produces tunable laser output over the 14 800–16 600 cm^{-1} range with a maximum power output of 150 mW. The standing wave 3-mirror dye laser contains a flat output coupler, OC, a curved fold mirror (f = 50 mm), FM, and a curved high reflector (f = 75 mm), HR. The operating wavelength of the dye laser is controlled with a tuning wedge, TW, located in a rotating mount attached to an xyz translation stage. The TW is mounted at Brewster's angle to minimize power losses. Tuning can be accomplished using three different approaches: rotation, vertical translation, and horizontal translation. The rotation of the TW through the Brewster's angle plane of the mount broadly tunes the laser and serves as the coarse adjustment to the operational wavelength range. It was found that rotating the TW so that the thickness gradient of the wedge is at ~45° from vertical produced the broadest spectral output. Vertical translations serve as an intermediate adjustment, and fine tuning of the laser is accomplished using horizontal translation of the TW. With this assembly, a single set of optics and two laser dyes (DCM and R6G) enabled the dye laser to be tuned from 585 to 675 nm using less than 2.50 W of pump power.

The dye laser output is passed through an extracavity I_2-cell before being directed through an acousto-optic modulator (AOM) and into a 2 m long Spex 2062 monochromator. The dispersed beam is then imaged onto a 1024-channel EG & G diode array detector, resulting in individual scans with spectral width of approximately 6 cm^{-1}. The spectral width is determined by the dispersion of the diffraction grating at a given order and the physical width of the diode array detector. The output from the detector is read using a GPIB board and software program OMA88. The dye laser is operated in an intentionally broadband ILS fashion using two AOMs with a pulse-and-delay generator. The timing sequence is monitored by directing a portion of the dye-laser output onto a photodiode connected to an oscilloscope. The first AOM is inline with the pump laser and dictates the total cycle time: at the start of the sequence, AOM1 is switched off and the pump beam is directed into the dye jet. Each sequence ends when AOM1 is switched on and diffracts the pump beam into a beam stop reducing the

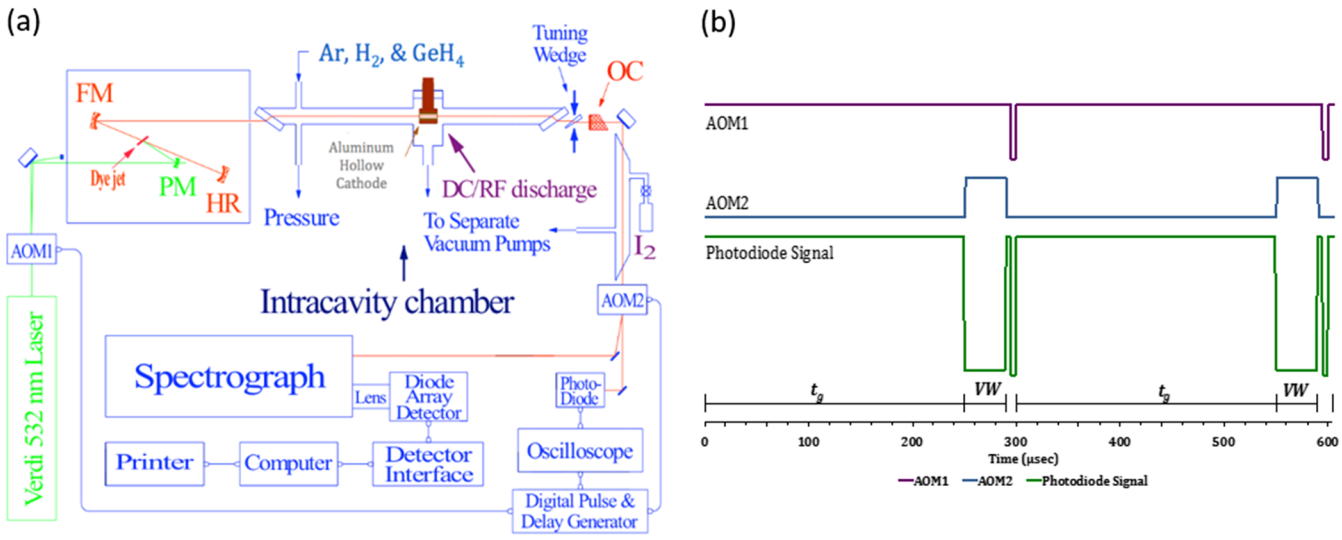

FIG. 1. (a) Schematic of the Intracavity Laser Spectrometer and (b) Timing sequence for two cycles of ILS operation, with the portion of the pump laser directed into the dye cavity by AOM1 shown in purple, the portion of the dye laser directed into the monochromator by AOM2 shown in blue, and the laser dye power output measured by a photodiode shown in green. During the generation time, t_g, molecular absorption is enhanced by the laser action as AOM1 is off during the "on" period of the laser and AOM2 directs dye laser output onto the photodiode, but not the monochromator. After t_g, for a time period termed the viewing window, VW, AOM2 directs a high percentage of the dye laser output into the monochromator, leading to a decreased intensity monitored by the photodiode. At the completion of the VW period, AOM1 diverts the pump laser so that the dye excitation is below the lasing threshold, terminating the dye laser output and resetting the system for the next cycle. For this study, a cycle time of 300 μs was used with a detector exposure window of 0.8 s, making each spectrum the sum of 2700 viewing windows.

pump power below the lasing threshold of the dye. The second AOM is used to set the effective path length and detector viewing window for operation of each cycle. During this period after dye laser initiation termed the generation time, t_g, any molecular absorbance will be enhanced by the laser action of the system. The effective path length, L_{eff}, can be determined with[17]

$$L_{eff} = c\, t_g \left(\frac{l}{L}\right), \tag{1}$$

where l is the region in the cavity occupied by the absorber (i.e., the length of the hollow cathode) and L is the length of the laser cavity. After t_g, the second AOM directs ~95% of the beam into the monochromator for the duration of the viewing window. For this study, a 150 mm long aluminum hollow cathode was installed in a 1.1 m long laser cavity, and the generation times used ranged from 50 to 200 μs, resulting in effective path lengths of 1.8–7.5 km. An illustration of the timing sequence used for the ILS process as observed by the photodiode is provided in Fig. 1(b).

To perform the intracavity spectroscopy measurements, a reaction chamber with two Brewster angle windows is located between the FM and TW optical components. The reaction chamber includes a hollow metal cathode for plasma formation. Ports to the reaction chamber include gas supply and exhaust valves, enabling variation in the gas flow and composition. The dye laser is aligned so that it passes through the hollow cathode, ensuring that any material formed in the plasma discharge around the cathode will be in the beam path. For this study, the reaction chamber was maintained at a total pressure of 800 mTorr with a gas mixture of 62.5% Ar, 25.0% GeH_4, and 12.5% H_2. All gas flows were regulated using MKS mass flow controllers.

The GeH molecules were produced in a plasma formed when a discharge current of 0.40–0.60 A DC was applied to an aluminum cathode. It was found that spectral features due to GeH were very strong when the plasma was initially engaged but faded quickly, while features due to GeH_2 grew as the discharge continued. Consequently, to maximize the GeH signal, it was necessary to record spectra as a single diode-array scan synchronized with plasma initiation, resulting in a relatively noisy background.

The spectrum of GeH between 16 000 and 16 600 cm^{-1} was collected as a series of overlapping ~6 cm^{-1} segments. Each spectral segment consisted of a spectrum collected of the plasma discharge, a spectrum collected in the absence of the plasma, and a spectrum from the external heated iodine cell used for calibration. Data processing and calibration are discussed in detail in Sec. II B.

The $a\,^4\Sigma^- – X\,^2\Pi_{1/2}$ transition of GeH was identified in the region between 16 000 and 16 600 cm^{-1}. The 15 000–15 550 cm^{-1} region was also investigated, but the $a\,^4\Sigma^- – X\,^2\Pi_{3/2}$ transition previously reported in that region[6] could not be identified in the observed data.

B. Data processing to produce a concatenated spectrum

The process used to produce a finalized spectrum can be summarized in four steps: conversion of the raw data into a transmission spectrum, calibration using iodine spectra, concatenating overlapping plasma spectral segments to form a single spectrum file, and the determination of spectral line positions from the obtained data.

1. Data conversion and calculation of derivatives

Data conversion and derivative calculation are performed with an in house Visual Basic program, ANEW. To produce a plasma spectrum for a given monochromator position, the baseline current (recorded when the laser was blocked by a beam stop) is subtracted from all data, then the plasma and I_2 spectra are divided by the background spectrum for the specific monochromator position, producing the transmission spectrum that is used for the analysis. The 1024-diode array channels are assigned tentative wavenumber positions from an empirically derived polynomial that correlates the order of the diffraction grating, a grating equation for the monochromator position, and the detector channel number to the vacuum wavenumber of the detected signal.[18] These initial assignments are typically accurate to ±0.1 cm^{-1}. Savitzky-Golay polynomials for the 1st and 2nd derivative of the transmission spectrum are then calculated, and text files are produced that contain the 1024 initial wavenumber positions, along with their corresponding transmission and 1st derivative and 2nd derivative values.

2. Calibration of iodine spectra using PGOPHER

The text files for the processed plasma and I_2 spectra are uploaded to PGOPHER[19] using the Overlay window option (see http://pgopher.chm.bris.ac.uk/Help/overlaying.htm for a walk-through of this process). Additionally, the supplementary material text file from the paper by Salami and Ross[20] that contains the transmission spectrum of I_2 from 14 250 to 20 000 cm^{-1} is uploaded. Both spectra must be inverted because peak assignments can only be made to peak maxima using PGOPHER. Narrow fully resolved experimental I_2 features were assigned to their corresponding peaks in the reference spectrum using the process outlined in the help section of PGOPHER's website (http://pgopher.chm.bris.ac.uk/Help/calibrating.htm). After peaks were assigned, the calibrated wavenumber positions and corresponding channel positions were fit to a 2nd order polynomial using PGOPHER's Calibration Window. Ten to thirty lines over approximately 6 cm^{-1} were selected from each I_2 spectrum for calibration depending on the quantity and quality of reference lines at a given monochromator position. The average deviation between the assigned reference I_2 line positions and calculated polynomial positions was typically ±0.002 cm^{-1}. Once the iodine files are calibrated, the dispersion polynomials obtained from the calibrations are applied to the corresponding plasma spectra. The individual calibrated plasma spectra can then be joined to create a single data file that contains all the experimental data collected at a constant set of conditions.

3. Merging of calibrated plasma files

The calibrated plasma files are concatenated using the "Join to. . ." feature of PGOPGHER Overlays. To form the

merged plasma file, two overlapping spectra are displayed on the PGOPHER screen, making sure that the plot area has a normalized and not an arbitrary vertical scale. The overlap region is then examined to find a location where the overlapping features are observed with similar intensity. Once this crossover point has been identified, the spectra are concatenated by right-clicking on the point and selecting "Join to…" from the popup menu. The next spectrum in the sequence is then displayed, and the overlap process is repeated until a single complete spectrum containing data for the entire spectral region investigated is obtained.

4. Calculation of line positions

After the merged plasma file has been produced, 1st and 2nd derivatives of the merged spectrum are calculated using the "Smooth" function of the PGOPHER Overlay window. The first derivatives were calculated using 2nd order Savitzky-Golay polynomials. In determining appropriate parameters for calculating the Savitzky-Golay 1st derivatives, it was found that using a large smoothing width resulted in inaccurate line positions for blended spectral features, so the minimum smoothing width of 5 data points was used. The 2nd derivatives were calculated using a 4th order Savitzky-Golay polynomial with a smoothing width of 9. As the 2nd derivatives were used to distinguish between molecular signals and random noise, a higher polynomial order and smoothing width were applied to reduce the magnitude of spurious fluctuations. To calculate peak positions, a set of Excel worksheets were created to identify zero-crossings in the 1st derivative data, determining the peak positions as the x-intercept for a line between the points on either side of the zero-crossing. The determined positions are then added to a text file that can be imported by PGOPHER as a linelist. For exceptionally noisy spectra, the number of zero-crossings in the 1st derivative data can be cumbersome and greatly reduce the utility of the linelist. In these cases, a threshold for "real" spectral features is estimated from the 2nd derivative data and used as a filter for reported line positions by only considering zero-crossings that correspond to 2nd derivative values exceeding this threshold.

III. RESULTS AND DISCUSSION

A. Branch assignment

A portion of the electronic spectrum of GeH is displayed in Fig. 2. The four branches for the $a\ ^4\Sigma^- – X\ ^2\Pi_{1/2}$ transition reported by Kleman and Werhagen,[6] the $^PQ_1$, $^QR_1$, $^PP_{21}$, and $^RP_{41}$ branches, were readily identifiable in the experimental data. The blue-degraded $^RP_{41}$ branch was somewhat difficult to identify because this branch overlaps the $0_0{}^0$ band of the $\tilde{A}\ ^1B_1 – \tilde{X}\ ^1A_1$ transition of GeH_2.[21] The molecular constants from Smith *et al.*[21] for $^{70}GeH_2$, $^{72}GeH_2$, $^{74}GeH_2$, and $^{76}GeH_2$ were used to produce a simulated spectrum for the transition to prevent possible assignment of GeH_2 features to GeH. Isotopologue structure was partially resolved in the $^PQ_1$ and $^PP_{21}$ branches for 4 germanium isotopes: ^{70}Ge, ^{72}Ge, ^{74}Ge, and ^{76}Ge, as can be seen in Fig. 3. Once these four branches were identified and assigned, a preliminary fit of the data was performed using PGOPHER.[19] Using the predicted branch structure from PGOPHER based on the initial fit, the four additional branches predicted to have appreciable intensity by Budo and Kovacs,[7] the $^QQ_{21}$, $^RQ_{31}$, $^sR_{31}$, and $^sQ_{41}$ branches, were identified and assigned in the experimental data. In total, 79 transitions were assigned to ^{70}GeH, ^{72}GeH, and ^{74}GeH. In all cases at low J ($J'' < 5.5$), the isotopologue splitting in the branches is too small to be fully resolved at the Doppler-limited resolution. However, in 5 of the 8 identified branches, at least 2 features are isotopically resolved. In total, 26 of the 79 assigned rotational transitions are isotopically resolved. The less abundant ^{76}GeH did not provide enough unique spectral features to justify a rotational analysis.

B. Obtaining molecular constants

Once branch assignments were obtained, the experimental data were fit to the Hamiltonian for $a\ ^4\Sigma^- – ^2\Pi_r$ transition using PGOPHER.[19] The $X\ ^2\Pi_r$ ground state constants were held fixed to the values provided by Towle and Brown[16] from their comprehensive fit of IR spectra for all isotopologues of GeH. Details of the Hamiltonian and the ground state parameters used for the fit are provided in the supplementary material. The spin-dependent interaction terms for Σ states of quartet and higher multiplicity used by PGOPHER were developed

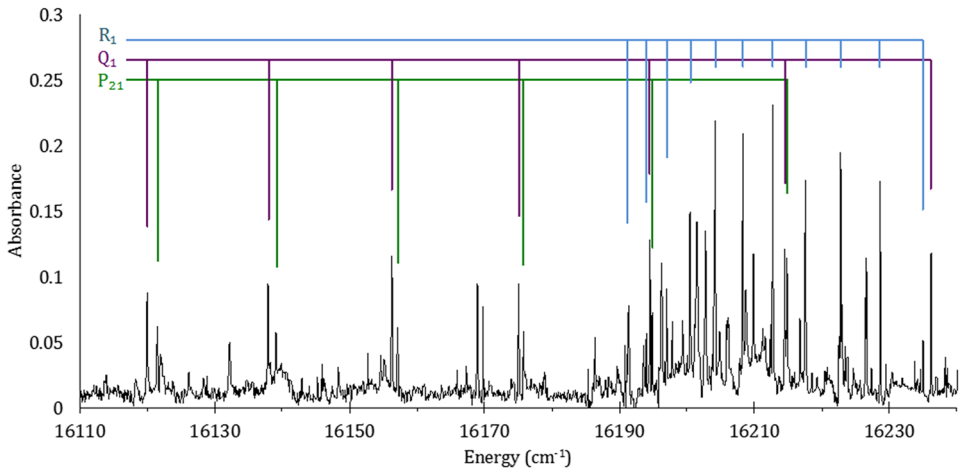

FIG. 2. Portion of the ILS spectrum of GeH observed in the dissociation of GeH_4 in a plasma. This image is a compilation of ~10 individually collected spectra. The R_1, Q_1, and P_{21} branches of the $a\ ^4\Sigma^- – X\ ^2\Pi_{1/2}$ transition of ^{74}GeH are indicated for clarity. Many of the unassigned features have been attributed to GeH_2 upon comparison with the work of Smith *et al.*[21]

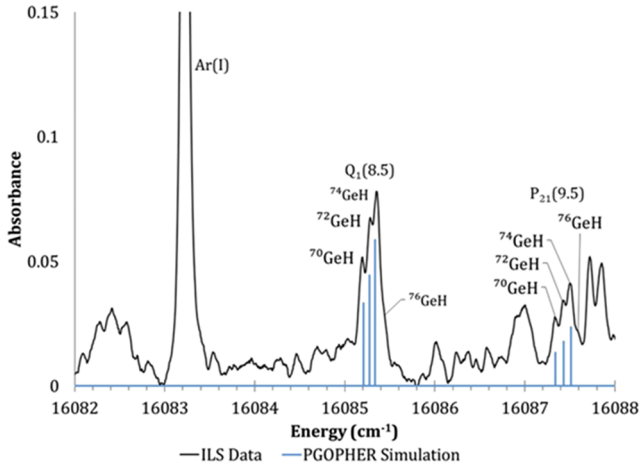

FIG. 3. Experimental plasma spectrum (converted to absorbance) of the $Q_1(8.5)$ and $P_{21}(9.5)$ lines of the $a\,^4\Sigma^- – X\,^2\Pi_{1/2}$ transition of GeH. Peaks due to ^{70}GeH, ^{72}GeH, and ^{74}GeH are clearly identifiable and have been highlighted in blue with simulated line positions from the PGOPHER[19] fit. There are weak shoulders due to ^{76}GeH to the blue of the main peak that are insufficiently resolved to justify analysis.

by Brown and Milton[22] based on the initial work of Hougen.[9] Hougen proposed that a Σ state with even multiplicity has S−½ spin-spin parameters and S+½ spin-rotation parameters. A $^4\Sigma$ state would then have one spin-spin parameter, λ_{SS}, and two spin-rotation parameters, namely, a first-order parameter, γ, and a third-order parameter, γ_S. For spectral features that were unblended and fully resolved, line positions were assigned using the 1st derivative zero crossings (*vide supra*) and were assigned an expected uncertainty of 0.005 cm^{-1} in the fit. Spectral features that were degraded but not fully resolved were assigned line positions manually and assigned an uncertainty of 0.01 cm^{-1}. Spectral features that were obscured or partially overlapped by GeH_2 features were assigned line positions as "best guesses" and given a statistical weight of 0.03 cm^{-1}. Of the 237 individual transitions included in the fit, 71 transitions were held to 0.005 cm^{-1}, 132 transitions were held to 0.01 cm^{-1}, and 34 were held to 0.03 cm^{-1}. For ^{74}GeH, 45 of the 79 transitions were held to 0.005 cm^{-1}, but just 18 transitions were fully resolved for ^{72}GeH, and only 8 transitions were fully resolved for ^{70}GeH. To fit the line positions of the ^{74}GeH $a\,^4\Sigma^- – X\,^2\Pi_{1/2}$ transition, it was necessary to include λ_{SS}, γ, and γ_S as well as a term energy (T), a rotational constant (B), a centrifugal distortion term (D), and a centrifugal spin-spin term (γ_D) in the PGOPHER $^4\Sigma^-$ Hamiltonian. In the fit of ^{70}GeH and of ^{72}GeH, γ_S was not determined within the experimental uncertainty due to the more limited number of resolved lines available for the less abundant isotopologues and, as a consequence, was held fixed to the value determined for ^{74}GeH. The results of the fit are shown in Table I; our results for ^{74}GeH are compared with results from the work of Kleman and Werhagen[6] and Klynning.[8] The line positions, assignments, and residuals are provided in tables in the supplementary material, along with the correlation matrix for the fit.

C. Interpretation of results

Results from the fit are in reasonable agreement with those from the work of Kleman and Werhagen[6] and Klyinning;[8] however, the values obtained in this study are determined to a much higher level of precision. Deviations between the values for parameters obtained in this study and the previously reported values that exceed the estimated standard deviations from the fit (reported in parentheses in Table I) not only are due to the quality of the experimental apparatus available in 1953 in comparison to present instrumentation but are also affected by slight differences in the Hamiltonian models used in the previous analyses.

The quality of the fit of the partially resolved isotope structure can be evaluated by comparing the ratios of the rotationally dependent parameters determined by the fit to the expected mass dependence of the parameters. The relationships between rotational constants and the reduced masses of the isotopologues were outlined by Dunham and summarized by Herzberg,[23]

$$B_e^i = \mu/\mu^i B_e, \tag{2}$$

$$D_e^i = \left(\mu/\mu^i\right)^2 D_e, \tag{3}$$

where the i superscript denotes the less abundant isotopologue, B_e values are equilibrium rotational constants, D_e values are equilibrium centrifugal distortion constants, and μ values are reduced masses of the isotopologues. Using these equations, the molecular constants for less abundant isotopologues can be calculated from corresponding constants for the more

TABLE I. Molecular constants for the $a\,^4\Sigma^-$ state of GeH (in cm^{-1}). Experimental values from other workers are shown in italics. Values in parentheses represent 1σ and are scaled to the last significant digit of the reported parameter.

$a\,^4\Sigma^-$ state	T_0	B_0	$D_0 \times 10^3$	λ_{SS}	$\lambda_D \times 10^3$	γ	$\gamma_S \times 10^3$	RMS[a]	N
^{70}GeH	16 751.9133(20)	6.769 116(50)	0.456 04(26)	9.7533(17)	0.373(29)	0.080 63(12)	−0.378[b]	0.0101	67[c]
^{72}GeH	16 751.7314(16)	6.767 009(44)	0.458 45(24)	9.751(14)	0.387(23)	0.079 24(11)	−0.378[b]	0.0078	69[c]
^{74}GeH	16 751.5529(13)	6.764 917(32)	0.459 66(16)	9.7448(11)	0.471(17)	0.077 934(81)	−0.378(75)	0.0060	67[c]
^{74}GeH[d]	*16 758.0*	*6.775*	*0.472*	*6.4*		*0.04*			
^{74}GeH[e]	*16 746.50(4)*	*6.755 4(5)*	*0.460(1)*	*6.51(2)*		*0.041(1)*	*−2.8(1)*	*0.1059*	*79*

[a] $\sqrt{\Sigma(Obs - Calc)^2/N}$.

[b] Held fixed to the value determined for ^{74}GeH.

[c] Line positions for obscured features that were bracketed by identified transitions were roughly approximated and held to 0.03 cm^{-1} in the fit. The deviations between the fit and these approximate values were omitted from the RMS calculation due to their somewhat arbitrary nature.

[d] Values from Kleman and Wehagen;[6] the zero-point energy of the $X\,^2\Pi_{1/2}$ state has been added to the term value provided in this reference.

[e] Values from Klynning;[8] the term energy from this reference has been modified so that the energy of the $X\,^2\Pi_{1/2}$ state is set to zero.

TABLE II. The B_0 and D_0 values (in cm^{-1}) for ^{70}GeH and ^{72}GeH obtained from the PGOPHER fit of the $a\,^4\Sigma^-$–$X\,^2\Pi_{1/2}$ transition of GeH are compared to values predicted from the Dunham equations and the experimental constants for ^{74}GeH. In the third column, deviations between the determined and predicted values are given in terms of 1σ.

$a\,^4\Sigma^-$ state	B_0 from fit			
^{74}GeH	6.764 917	(32)	Calculated B_0 from ^{74}GeH Value	(Fit-calc)/(σ_{Fit})
^{72}GeH	6.767 009	(44)	6.767 446	−9.93
^{70}GeH	6.769 116	(50)	6.770 118	−20.04
	$D_0 \times 10^3$ from fit			
^{74}GeH	0.000 459 66	(16)	Calculated $D_0 \times 10^3$ from ^{74}GeH value	(Fit-calc)/(σ_{Fit})
^{72}GeH	0.000 458 45	(24)	0.458 65	−6.47
^{70}GeH	0.000 456 04	(26)	0.459 01	−16.64

abundant isotopologue. Because ^{74}GeH is 1.32 times more abundant than ^{72}GeH and 1.75 times more abundant than ^{70}GeH, more transitions can be assigned to ^{74}GeH than to the less abundant isotopes and many line positions assigned to these weaker features can be skewed slightly by the close-lying transition of the more abundant isotopologue. To assess the quality of the fit determined for ^{70}GeH and ^{72}GeH, the values determined from the fit for B and D are compared to the values calculated using Eqs. (1) and (2) in Table II. One standard deviation for the parameter from the fit is given in parentheses, and the deviation between the determined and calculated value has been scaled to match these values. As is to be expected, the magnitude of deviations from the calculated values for ^{70}GeH are larger than those for ^{72}GeH. While both determined B and D values agree moderately with the expected isotopologue shift, the deviations are larger in scale than the reported uncertainties from the fit. This could be because the comparison values are specific to v = 0 and Eqs. (1) and (2) are only rigidly descriptive for equilibrium values,[23] or the deviations could be due to the limited data for the lighter isotopologues. In most cases, isotopologue splitting was not observed below $J'' = 5.5$, which is already 237 cm^{-1} above the ground state. The observed transition with the highest ground state rotational momentum was the $^qR_1(16.5)$, excited from a state 1915 cm^{-1} higher than the ground state and only intense enough to be observed because the isotopologues have yet to separate in this branch. During data acquisition, it became clear that gentle discharge conditions enhanced the GeH signal, while more intense discharge conditions favored the formation of GeH_2. As a consequence, a more energetic discharge did not always result in a more intense GeH absorption signal from high J'' transitions due to the enhancement of overlapping GeH_2 peaks. This is likely the reason that no $a\,^4\Sigma^-$–$X\,^2\Pi_{3/2}$ transitions were observed, which lie in a region of strong GeH_2 signal.[16]

A recent computational paper[1] suggested that discrepancies between experimental constants for the $a\,^4\Sigma^-$ state and their computational counterparts required more precise experimental data to adequately evaluate the quality of the different computational approaches used to model the lowest $^4\Sigma^-$ state of GeH. The experimental T_0, B_0, D_0, and r_0 values are compared to the reported computational values from Refs. 1–3, and 5 in Table III. When α_e values were not determined, B_e, D_e, and r_e values are used instead of v = 0 values. The T_0 values evaluate the combined accuracy of the excitation energy and vibrational frequency. The B_0 and r_0 values evaluate the accuracy of the calculated bond length, and the D_0 values evaluate the combined accuracy of the bond length and

TABLE III. Comparison of experimentally derived parameters (in cm^{-1}) and their computational counterparts for the $a\,^4\Sigma^-$ state of ^{74}GeH.

$a\,^4\Sigma^-$ state of ^{74}GeH	T_0	B_0	$D_0 \times 10^3$[a]	r_0 (Å)
Experiment	16 751.5524	6.764 912	0.459 60	1.5831
Li *et al.* 2015[1]				
MRCI + Q and core-valence effect	16 644.98	6.8744	0.489 95	1.570
MRCI + Q, no core-valence effect	16 696.77	6.8519[b]	0.340 6[b]	1.573[b]
Li *et al.* 2013[5 c]				
CCSD(T)/CBS	16 800.65	6.976[b]	0.390 1[b]	1.559[b]
Bruna and Grein 2001[3]				
MRCDI/full CI	15 069.5	6.806[b]	0.398 0[b]	1.578[b]
Balasubramanian and Li 1988[2]				
MCSCF (CAS SCF)+CI	14 732.5			

[a]Calculated using the Kratzer Relationship $D = 4B^3\omega^{-2}$.
[b]Values represent equilibrium constants.
[c]Excitation Energy and Bond Length from the CCSD(T)CBS, Harmonic frequency from the CCSD(T)/cc-pV5Z level of theory.

vibrational frequency. The term energy is best predicted by the coupled-cluster single and double excitation with perturbative triples at the complete basis set limit [CCSD(T)/CBS] method from Li *et al.*[5] and the multi-reference configuration interaction with the Davidson correction (MRCI+Q) method without the Core-Valence Effect from Li *et al.*,[1] both accurate within 60 cm^{-1} of the observed value. The inclusion of the Core-Valence Effect actually resulted in a comparable but slightly worse description of the system. The level of agreement between the predicted T_0 and determined excited state energy strongly suggests the excited state vibrational assignment as $v' = 0$, which is confirmed experimentally by a very small shift in transition energy for the GeH isotopologues. Differences between predicted bond lengths and the derived value from the experimental B_0 values were all in reasonable agreement, the worst being the CCSD(T)/CBS method of Li *et al.*[5] with a percent difference of −1.52% from the determined value. No method predicted the centrifugal distortion constant particularly well, but the best case was the MRCI+Q and Core-Valence Effect method of Li *et al.*[1] with a percent difference of 6.6% from the determined value. This is likely due to the reliance of the computational values provided in Table III upon the Kratzer relationship[23] and reported B_e and ω_e values, rather than a direct computational determination of the centrifugal distortion effects.

The spin-spin parameter, λ_{ss}, is expected to have a direct contribution from spin-spin dipolar interactions and a second order spin-orbit contribution that results from interactions with nearby states with the same electron configuration.[24] The $a\ ^4\Sigma^-$, $A\ ^2\Delta$, and $1\ ^2\Sigma^+$ states arise from the $8\sigma^2 9\sigma^1 4\pi^2$ configuration.[1] The isoconfigurational second order contribution to λ_{ss} and $\lambda_{SO,}$ can be estimated using the relationship for a $\sigma\pi^2$ configuration from Lefebvre-Brion and Field,[25]

$$\lambda_{SO} = \frac{1}{6}\frac{\left[A(^2\Pi, \sigma^2\pi\right]^2}{E(^2\Sigma^+) - E(^4\Sigma^-)}, \tag{4}$$

where, for GeH, $A(^2\Pi,\sigma^2\pi)$ is the spin-orbit splitting of the $8\sigma^2 9\sigma^2 4\pi^1\ X\ ^2\Pi_r$ ground state, reported to be 893 cm^{-1} by Towle and Brown,[16] $E(^2\Sigma^+)$ is computed to be 32 293 cm^{-1} by Li *et al.*,[1] and $E(^4\Sigma^-)$ is determined to be 15 810 cm^{-1} in this work. The resulting λ_{SO} of 8.05 cm^{-1} is of similar magnitude to the determined λ_{ss} value of 9.75 cm^{-1} and indicates that the direct spin-spin interaction in the $a\ ^4\Sigma^-$ state is quite small.

IV. CONCLUSIONS

An intracavity dye-laser absorption spectrometer has been used to record the absorption spectrum of the spin-forbidden $a\ ^4\Sigma^-$–$X\ ^2\Pi_{1/2}$ transition of GeH. Isotopologue structure was observed, and a rotational analysis was performed on transitions of the three most abundant isotopologues: ^{70}GeH, ^{72}GeH, and ^{74}GeH. The obtained rotational constants for the less abundant isotopes are found to be in reasonable agreement with the values predicted from the Dunham equations. The vibrational assignment of this transition, which was ambiguous in the initial report, has been assigned as the (0-0) band due to the magnitude of the isotopic shift and the strong agreement between theory and experiment.

SUPPLEMENTARY MATERIAL

See supplementary material for Hamiltonian elements used by PGOPHER;[19] ground state constants for the $X\ ^2\Pi_r$ state from Towle and Brown[16] that were used in the fit; line positions, assignments, and residuals for the fit of the $a\ ^4\Sigma^-$–$X\ ^2\Pi_{1/2}$ transition of GeH; and the correlation matrices for parameters associated with the fit.

ACKNOWLEDGMENTS

This work was supported by the National Science Foundation, Grant Nos. CHE-1566454(JOB) and CHE-1566442(LOB). The authors would like to acknowledge Sigma-Aldrich for the donation of the GeH_4 lecture bottle.

[1] R. Li, Z. Zhai, X. Ziang, M. Jin, H. Xu, and B. Yan, J. Quant. Spectrosc. Radiat. Transfer **157**, 42 (2015).
[2] K. Balasubramanian and J. Li, J. Mol. Spectrosc. **128**, 413 (1988).
[3] P. J. Bruna and F. Grein, J. Mol. Struct. **599**, 261 (2001).
[4] C. Song, T. Gao, H. Ham, M. Wan, and Y. Yu, J. Mol. Struct.: THEOCHEM **870**, 65 (2008).
[5] H. Li, H. Feng, W. Sun, Y. Xie, and H. F. Schaefer, Inorg. Chem. **52**, 6849 (2013).
[6] B. Kleman and E. Werhagen, Ark. Fys. **6**, 399 (1953).
[7] A. Budo and I. Kovacs, Z. Phys. **116**, 693 (1940).
[8] L. Klynning, Ark. Fys. **32**(34), 563 (1966).
[9] J. T. Hougen, Can. J. Phys. **40**, 598 (1962).
[10] J. M. Brown, K. M. Evenson, and T. J. Sears, J. Chem. Phys. **83**, 3275 (1985).
[11] J. P. Towle and J. M. Brown, Mol. Phys. **70**(1), 161 (1990).
[12] W. Zimmermann, K.-P. Smolka, and W. Urban, Mol. Phys. **70**(1), 167 (1990).
[13] Y. Akiyama, K. Tanaka, and T. Tanaka, J. Chem. Phys. **94**(4), 3280 (1991).
[14] M. Petri, U. Simon, W. Zimmermann, W. Urban, J. P. Towle, and J. M. Brown, Mol. Phys. **72**, 315 (1991).
[15] G. Huhn, U. Simon, M. Petri, W. Zimmermann, and W. Urban, Mol. Phys. **76**, 1029 (1991).
[16] J. P. Towle and J. M. Brown, Mol. Phys **78**(2), 249 (1993).
[17] B. Kalmar and J. J. O'Brien, J. Mol. Spectrosc. **192**, 386 (1998).
[18] L. C. O'Brien, H. Cao, and J. J. O'Brien, J. Mol. Spectrosc. **207**, 99 (2001).
[19] PGOPHER, a program for simulating rotational, vibrational and electronic spectra, C. M. Western, J. Quant. Spectrosc. Radiat. Transfer **186**, 221–242 (2016).
[20] H. Salami and A. J. Ross, J. Mol. Spectrosc. **223**(1), 157 (2005).
[21] T. C. Smith, D. J. Clouthier, W. Sha, and A. G. Adam, J. Chem. Phys. **113**(21), 9567 (2000).
[22] J. M. Brown and D. J. Milton, Mol. Phys. **31**(2), 409 (1976).
[23] G. Herzberg, *Molecular Spectra and Molecular Structure. I. Spectra of Diatomic Molecules* (D. Van Nostrand, Princeton, NJ, 1950), p. 143.
[24] T. Nelis, J. M. Brown, and K. M. Evenson, J. Chem. Phys. **92**, 4067 (1990).
[25] H. Lefebvre-Brion and R. W. Field, *The Spectra and Dynamics of Diatomic Molecules* (Elsevier, San Diego, CA, 2004), pp. 199–201.